MOLECULAR CANCER THERAPEUTICS | MODELS AND TECHNOLOGIES



Li Wan¹, Jun Yin², John Skoko³, Russell Schwartz⁴, Mei Zhang², Philip R. LeDuc¹, and Carola A. Neumann³

ABSTRACT

Disease models, including *in vitro* cell culture and animal models, have contributed significantly to developing diagnostics and treatments over the past several decades. The successes of traditional drug screening methods were generally hampered by not adequately mimicking critical *in vivo* features, such as a 3D microenvironment and dynamic drug diffusion through the extracellular matrix (ECM). To address these issues, we developed a 3D dynamic drug delivery system for cancer drug screening that mimicks drug dissemination through the tumor vasculature and the ECM by creating collagen-embedded microfluidic channels. Using this novel 3D ECM microsystem, we compared viability of tumor pieces with traditionally used 2D

methods in response to three different drug combinations. Drug diffusion profiles were evaluated by simulation methods and tested in the 3D ECM microsystem and a 2D 96-well setup. Compared with the 2D control, the 3D ECM microsystem produced reliable data on viability, drug ratios, and combination indeces. This novel approach enables higher throughput and sets the stage for future applications utilizing drug sensitivity predicting algorithms based on dynamic diffusion profiles requiring only minimal patient tissue. Our findings moved drug sensitivity screening closer to clinical implications with a focus on testing combinatorial drug effects, an option often limited by the amount of available patient tissues.

Introduction

Advancements in drug screening build off a substantial body of work with ex vivo cell culture models on 2D systems [96-well plates, gelatin sponge, etc. (1, 2)]. Although these approaches are powerful, they often resemble physiologic relevant environments (3). Therefore, building 3D microenvironments that better mimic in vivo conditions has been of great interest (4-6). Part of these advances is the development of microfluidic systems for vasculature (7-9). Advancements in drug circulatory diffusion were developed with microfluidic systems to replicate the surrounding tumor vasculature (7–9). Polydimethylsiloxane (PDMS) is often used as a primary material for microfluidic chip fabrication due to its flexibility and high gas permeability. However, PDMS does not form a biocompatible extracellular matrix for 3D cell culture, but rather serves as an inorganic substrate that lacks physiologic features (10, 11) of biomaterials of the ECM, such as collagen type I (12). In addition, PDMS has a strong hydrophobic nature that causes hydrogen bonding or pola-polar interactions negatively influencing drug diffusion (13).

Collagen makes up approximately 30% of protein in the body, while PDMS does not exist in the body. Thus, combining microfluidic

¹Department of Mechanical Engineering, Carnegie Mellon University, Pittsburgh, Pennsylvania. ²Department of Developmental Biology, University of Pittsburgh Medical Center Cancer Institute, Magee Womens Research Institute, Pittsburgh, Pennsylvania. ³Department of Pharmacology and Chemical Biology, University of Pittsburgh Medical Center Cancer Institute, Magee Womens Research Institute, Pittsburgh, Pennsylvania. ⁴Computational Biology Department, Carnegie Mellon University. Pittsburgh, Pennsylvania.

Note: Supplementary data for this article are available at Molecular Cancer Therapeutics Online (http://mct.aacrjournals.org/).

Corresponding Authors: Carola A. Neumann, Pharmacology and Chemical Biology, University of Pittsburgh Cancer Institute, Pittsburgh, PA 15213. Phone: 412-641-7725; E-mail: neumannc@upmc.edu; and Philip R. LeDuc, Department of Mechanical Engineering, Carnegie Mellon University, Pittsburgh, PA 15213. Phone: 412-268-2504; Fax: 412-268-3348; E-mail: prl@andrew.cmu.edu

Mol Cancer Ther 2021;20:1210-9

doi: 10.1158/1535-7163.MCT-20-0880

©2021 American Association for Cancer Research.

collagen-embedded channels with techniques such as sacrificial template molding (14) and 3D bioprinting (15, 16) provides advantages that close the gap between *ex vivo* cell culture models and animal models. Clearly, animal models provide much greater physiological relevance but are less cost effective and can yield responses relevant to animals but are unintentionally misleading in humans (17, 18). Importantly, animal models often lack immune system functionality (19) and species-specific drug response (19, 20) thus, presenting inconsistent responses compared to clinical trials in human patients (21).

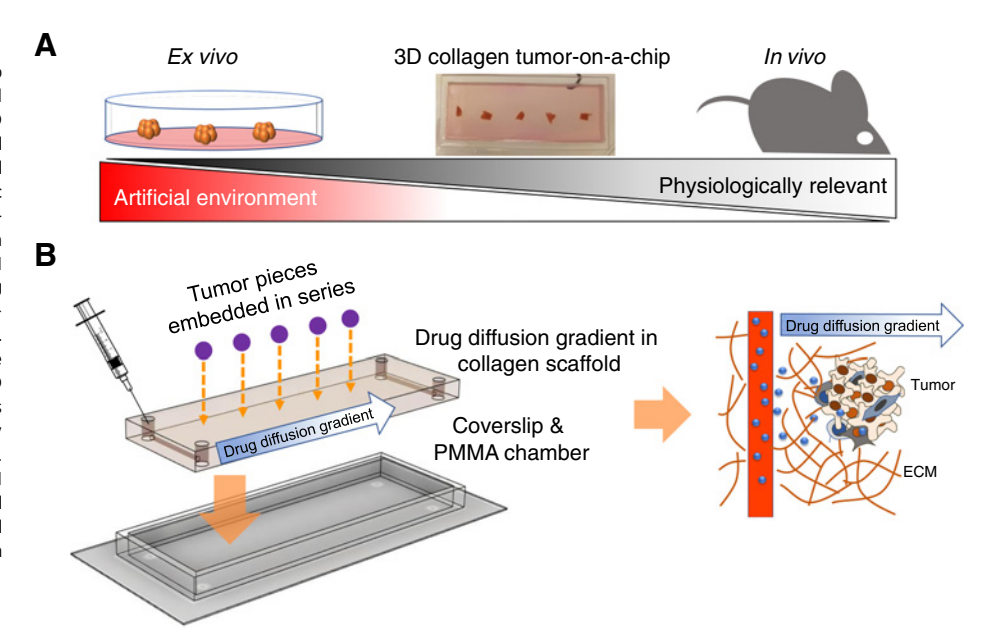
Several tumor-on-a-chip models have been developed in recent years to overcome limitations of exsiting techniques. For example, Chang and colleagues (22) developed a PDMS-based drug screening device on 96-well plates to test xenograft mouse brain tissues. Although this device offered a high-throughput design compared with traditional 2D drug screening, the systems were made of nonphysiological PDMS. Skardal and colleagues (23) developed a metastasis-on-a-chip model in which metastatic tumor cell migration was demonstrated in a circulating microfluidic system that connected a gut organoid with a liver organoid in two independent chambers. Although this approach mimicked in vivo conditions with more complexity, it still utilized an external PDMS-based microfluidic system. Other material-based approaches such as hydrogels have been used but not with respect to drug screening. Kolesky and colleagues (24) created microfluidic channels in gelatin and fibrinogen using 3D bioprinting, and Nguyen and colleagues (25) fabricated channels in collagen type I with 400-µm needles and coated the channel with endothelial cells. These designs introduced ECM embedded channels toward drug screening applications, but the 3D printing method was limited by channel resolution (26), and the use of needles was not extendable to more complex channel designs.

Here, we tested a 3D ECM microsystem that provides spatial, temporal and biological controlled microenvironment that resembles *in vivo* circulatory diffusion dynamics, which can greatly enhance the ability of tumor drug screening approaches as it mimics the *in vivo* tumor environment (TME; **Fig. 1A**). Five tumor pieces (1 mm³ in size) were placed next to opposing channels (0.5 mm) and aligned with the direction of the diffusion and drug gradient. This set-up allows the implementation of diffusion simulation in an ECM-resembling



Figure 1.

3D collagen vascular tumor-on-a-chip mimetics for dynamic combinatorial drug screening. A, A microfluidic 3D ECM-based drug screening device could fill the gap between ex vivo models and animal models, with more physiologic relevance compared with ex vivo models, and more direct controllability than animal models. B, Design of a 3D ECM based dynamic tumor-on-a-chip drug screening device. Tumors were positioned between two parallel channels. Microfluidic channels on both ends were available for drug perfusion. The 3D dynamic diffusion approach (left) was designed to mimic in vivo drug delivery from blood vessels to tumors (right). Drug molecules were perfused into ECM embedded microfluidic channels, and then the molecules physically diffused into ECM, generating a drug gradient in the scaffold.



scaffold, provides temporal and importantly, spatial control any 2D systems lacks. In addition, this 3D ECM microsystem allows for higher throughput, along with ease of manipulation for combinatorial drug dosing supported by simulation modelling to interpret responses to combinatorial dosing.

Results

3D ECM microsystem design and validation

Intravenous drug delivery from the vasculature into local tissue depends on diffusion profiles of the individual compounds. To replicate this process, we created a 3D collagen type I scaffolding in which five tumor tissues (1 mm³, derived from MDA-MB-231 human breast cancer cell line mouse xenografts) could be embedded (Fig. 1B). We previously developed a micromilling technique to fabricate microfluidic channels directly in a 3D ECM microsystem (14). Circular microfluidic channels were incorporated on both ends to establish drug gradients that perfuse across the device and the tumor samples (Fig. 1B). First, the clinically relevant breast cancer therapeutic drug adriamycin (doxorubicin; ref. 27) was tested to assess whether drug diffusion can be reliably predicted in the 3D-collage scaffold. Doxorubicin (30 µL) was injected into the left channel of the device and allowed to diffuse into the collagen scaffold for 24 hours. As doxorubicin molecules are autofluorescent (28), direct determination of the diffusion was determined through confocal microscopy imaging (Fig. 2A). Doxorubicin fluorescent signals were captured and intensity profiles were measured at 1 and 24 hours. After 24 hours (Fig. 2B), an approximately linear concentration profile was obtained from the left to the right channel. This allowed a one-dimensional simulation using Matlab, by applying Fick's second law in one dimension (1D), with the finite difference method as a simplified math model. The obtained diffusion profile was compared to a mathematically simulated diffusion profile predicted through diffusion equations as described (29, 30). Notably, experimentally obtained values for the slope of the curve were not significantly different from mathematically modeled curves (Fig. 2C). To further examine the accuracy of the 1D simulation in the 3D collage scaffold, the rhodamine 6G diffusion profile was predicted by using rhodamine 6G diffusion coefficients (31, 32) and comparing these modeling results with experimentally obtained values (Supplementary Fig. S1). Reassuringly, the 6G rhodamine diffucion profile matched the simulation as well.

To test the next drug responses of actual tumor tissues in the device, human breast tumor xenograft fragments were created by injecting MDA-MB-231 cells into nude mice (33). Tumor fragments were were dissected into two pieces (1 mm³) and characterized for viability to exclude dead tissue samples (Supplementary Fig. S2) prior to screening. 3D ECM microsystems were prepared with DMEM + 10% FBS to provide tumor samples with essential nutrients. To first examine tumor tissue survival over time, tumor tissue viability was examined up to 6 days with five tumor samples per device. Tumor samples were then analyzed with a live/dead stain (CalAM and EthD-1) and confocal microscopy (Fig. 2D and E). To avoid autofluorescence from tumor tissue, its ECM, and the collagen scaffold (34-36) to alter the analysis two methods where used to determine cell viability (Supplementary Fig. S3). First, because tumor autofluorescence is rather uniform throughout the tumor, image processing software was used (ImageJ bundled with Java 1.8.0_172; https://imagej.nih.gov/ij/download. html) to subtract autofluorescence from tumor tissue images. Second, tumors were cut into smaller pieces, gently manually detached with tweezers and against the coverslip. That way, it was found that tumor samples maintained over 75% viability in the device compared to initial viability of the tumor being approximately 80% (Fig. 2D). To get a better sense if tumor viability in the 3D ECM microsystem differs from the one found in conventional 1D methods, tumor pieces were seeded in a 96-well plate, immersed in media, and analyzed in parallel. As Fig. 2E shows, tissue viability varied from about 76% to 95% in both methods, but was comparable over time (Fig. 2E).

Single drug screening

To better mimic dynamic *in vivo* diffusion profiles and to identify drug concentrations that would fit best with COMPUSYN algorithms (37, 38), drug concentration simulation was used through Matlab coding to compare one-time dosing vs. constant-flow dosing (replenish drugs every 12 hours) over 3 days (Supplementary Fig. S4). The one-fill mode will cause a drop of initial high dose at the left

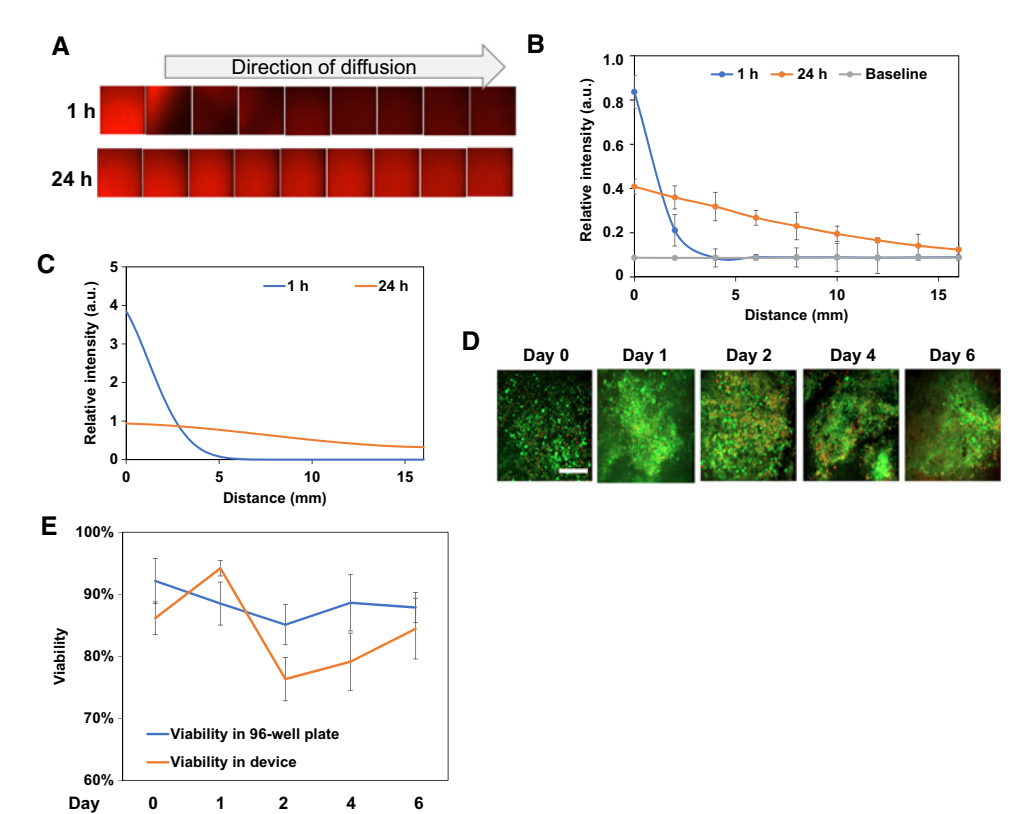


Figure 2. Diffusion profiles and cell viability in our ECM-based systems. A. A doxorubicin diffusion profile was captured through confocal microscopy imaging of doxorubicin fluorescent intensity at 1 and 24 hours. B. Quantification of doxorubicin diffusion for 1 and 24 hours. The gray line was the baseline fluorescence intensity without the presence of doxorubicin. C. 1D simulation of doxorubicin diffusion profile generated by applying the diffusion coefficient of doxorubicin from literature data. The simulation was similar to experimental results for the 1- and 24-hour diffusion profiles **D,** Viability tests for tumor samples cultured in 96-well plates and in our ECM tumor-on-a-chip device. E. Live/dead staining of tumor samples from day 0 to day 6, in 96-well plates and in our device. Scale bar, 200 μm.

channel, and the multiple-fills mode will cause a continuous increasing dose over the whole device. The constant-flow dosing mode suggested that compared to one-time dosing, higher max/min dose differences occur especially after 72 and 48 hours compared with 24 hours, which is preferable for more accurate simulation and estimation of a doseeffect curve using COMPUSYN.

To next correlate simulation with tumor viability, five tumor samples were placed in the 3D collage scaffold and 30 µL of media containing 100 µmol/L of doxorubicin was introduced into the left channel. To achieve a constant channel drug concentration and match the simulation of constant-flow mode, drug-containing media was replenished every 12 hours. As a control, five tumor samples were placed individually in 96-well plates, and treated directly with 100- μ L media (DMEM + 10% FBS) with doxorubicin (every 12 hours) doses corresponding to a 48-hour drug concentration simulated by Matlab for each tumor piece in the 3D device (Fig. 3A). The 48-hour drug concentration was chosen to create a comparable dosing scheme between the two devices. After 3 days, all 10 samples (device and 96-well plate) were analyzed by live/dead staining and tissue viability was determined (Fig. 3B). As expected, a dose-dependent decrease in viability that correlated with the drug dose gradient was observed in both 2D controls as well as 3D ECM microsystem. Notably, the 3D ECM microsystem samples showed lower viability compared to 2D controls. As a reference, tumor samples from the 3D ECM microsystem were also analyzed for proliferation and apoptosis by immunofluorescence staining for Ki-67 and caspase-3, respectively (Fig. 3C). As expected, a dose-dependent increase in Ki-67 (proliferation) and decrease in caspase-3 (apoptosis) was observed, which was quantified and consistent with the live/dead staining results (Fig. 3D). Doxorubicin intrinsic fluorescence decreased as well across the spatially distributed samples, which correlated with the drug simulation analysis (Fig. 2A-C).

Tumor viability during combination treatment

Drug synergism is an essential determinant in evaluating drug combination therapies. The advantage of syngergistic drug effects, when compared with additive effects, is that a specific drug ratio generates higher effects than the combined individual drug responses (additive). Thus, drug synergism is a desired factor in evaluating combinatorial drug schemes. The Chou-Talalay method (39) is frequently used to determine if two drugs act syngergistic, additive, or antagonistic. This method uses the combination index (CI) as a readout. Here, CI values, where CI < 1 marks synergistic, CI = 1 additive and CI > 1 antagonistic drug effects, were calculated using COMPUSYN software that is based on the Chou-Talalay method (39). The power of this method lies in determining optimal (less toxic) and efficacious drug ratios for combination treatments. In general, CI analyses are done in vitro using cell lines that allow testing of many different drug concentrations, but often lack in vivo reproducibility.

To test the feasibility of the 3D ECM microsystem, a drug combination was chosen that is commonly used to treat breast cancer: doxorubicin and cyclophosphamide act synergistically to kill tumor cells through different mechanisms (40). Doxorubicin kills cells by intercalation of DNA, topoisomerase II inhibition and free radical formation (41, 42). Cyclophosphamide metabolites (e.g., 4-hydroxycyclophosphamide) mediates cell death by alkylating and crosslinking DNA in cancer cells (41, 43-45). Four sample setups were used as illustrated in Supplementary Fig. S5 to analyze the known synergistic effect of both drugs in the 3D ECM microsystem: doxorubicin alone (denoted as doxo), 4-hydroxycyclophosphamide alone (denoted as

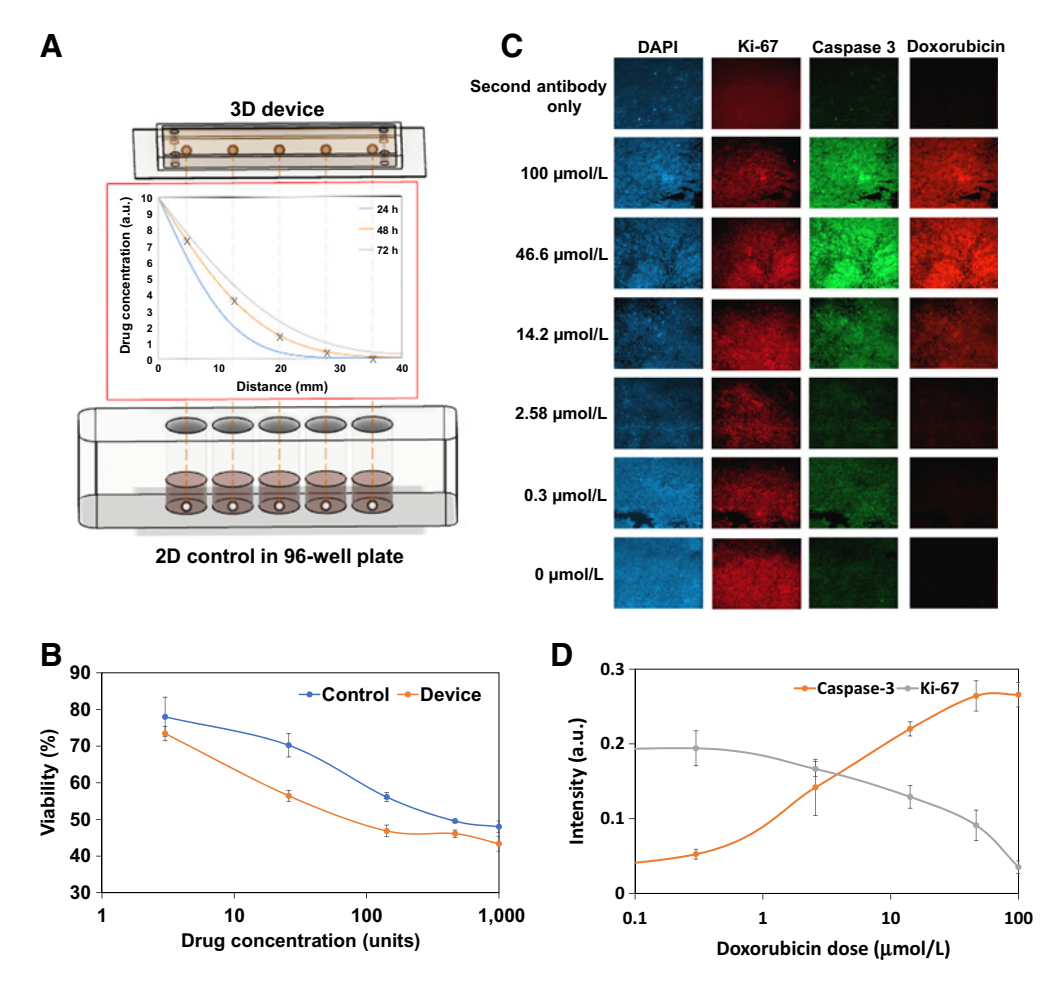


Figure 3. Tumor-on-a-chip response to single drug exposure. **A,** 3D devices versus 2D controls setup. Top: five tumors were inserted in series into the system. Middle: simulation of drug diffusion profile for 24, 48, and 72 hours. Bottom: In a 2D control, tumors were cultured in 96-well plates and treated directly with constant drug doses equal to the drug dose in the 3D device at 48 hours. **B,** Doxorubicin drug screening results for the device and control. Note that both presented similar trends, yet the absolute drug effect was different. For doxorubicin, 1,000 units = $100 \, \mu$ mol/L. Experiments were done in triplicates. **C,** Immunofluorescent staining for DAPI, Ki-67, and caspase-3, and autofluorescence of doxorubicin, in tumor samples treated with doxorubicin. Expression of caspase-3 increased and Ki-67 decreased with higher dosing, which agreed with the live/dead staining results. All images are $700 \times 700 \, \mu$ m. **D,** Quantification of immunofluorescent staining intensity of caspase-3 and Ki-67. The lines are polynomial interpolations.

cyclo), doxorubicin and 4-hydroxycyclophosphamide in opposite directions (denoted as oppo), and both drugs diffusing in the same direction (denoted as para for parallel). For oppo, doxorubicin and 4-hydroxycyclophosphamide were injected from the left and right channels, respectively; and for para, both drugs were injected from the left channel. Similar to the one-drug screening approach, 96-well controls were prepared, with drug doses matching 48-hour dosing in the 3D ECM microsystem (Supplementary Fig. S5). In the 3D device, the concentration of the drugs at each tumor sample location was again determined through 1D simulation as before (Supplementary Fig. S6A). The simulations revealed that compared with doxorubicin, 4-hydroxycyclophosphamide (277g/mol) diffused faster than doxorubicin (543 g/mol), as expected with its lower molecular weight (Supplementary Fig. S6B). Based on this and the median effect dose (Dm) of doxorubicin being previously reported as much lower than 4-hydroxycyclophosphamide for MDA-MB-231 cell treatment (46), we selected 100 µmol/L of doxorubicin and 100 mmol/L of 4-hydroxycyclophosphamide as the initial injection dose for each channel. Single drug treatments showed reduced tumor viability (one-effect; Supplementary Fig. S7A and S7B, where viability is one-effect) as the drug dose increased in the 96 well control and 3D ECM microsystem (Fig. 4C and D, blue and red lines).

As expected, treatment with both drugs at the same time in para showed lower tumor tissue viability than either of the single drugs alone, which indicated that the addition of either drug increased the overall effect (Fig. 4A top, 4C and 4D, gray lines). In both oppo treatment schemes, 2D and 3D, the tissue viability after drug combination was dominated by the highest dose of doxo (Fig. 4A bottom, 4E and 4F, gray lines). For the 3D ECM microsystem this suggests that the initial increase in tissue viability was due to a rapid drop of the dominating doxo effect, and that the subsequent decrease was mainly caused by synergistic combination effect of doxo and cyclo. The tissue viability curve (for both 2D control and 3D device) fluctuated from one side to the other, and reached a local minimum at double median dosing in the 3D ECM microsystem.

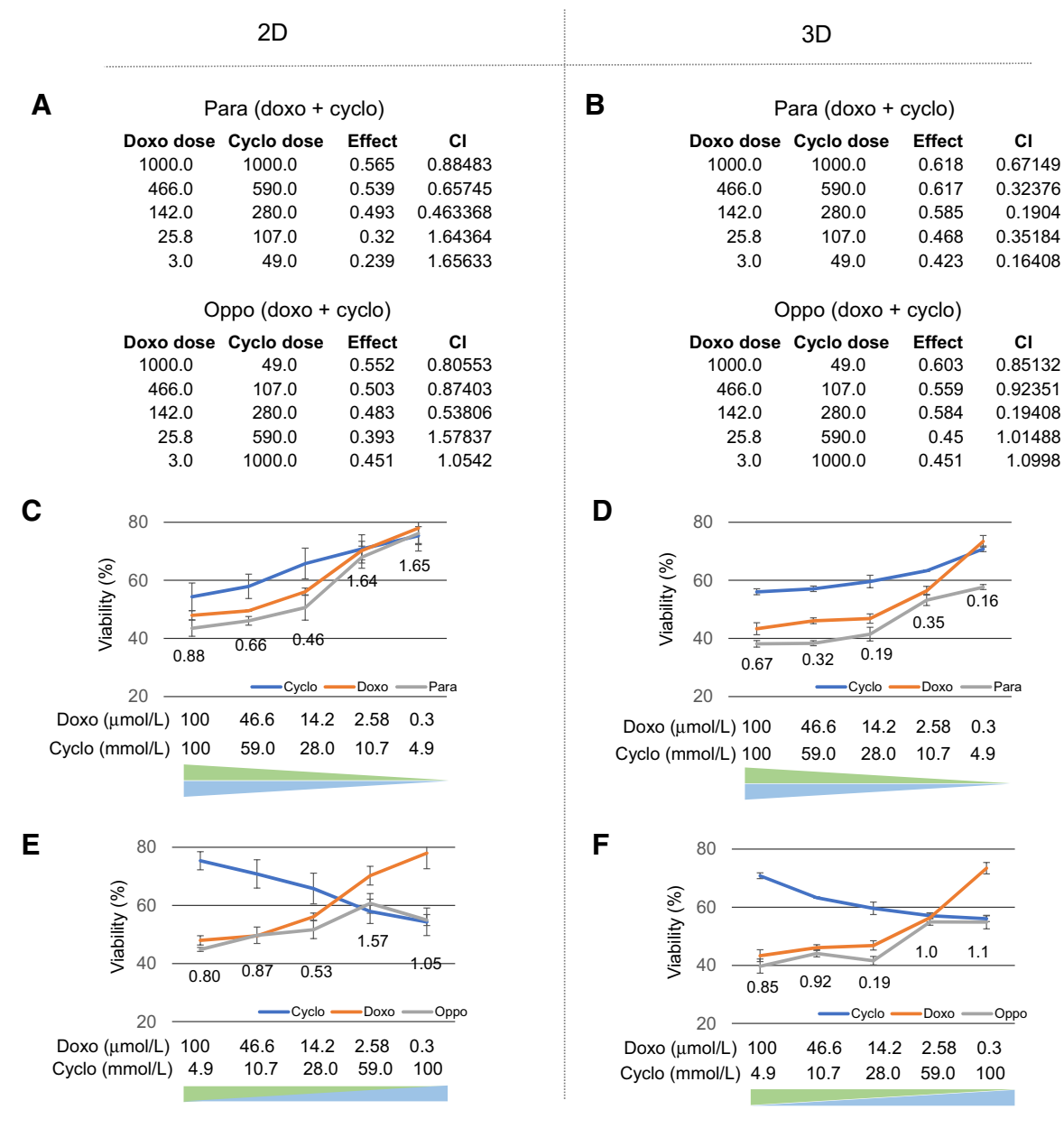


Figure 4.

Double drug screening with doxorubicin (doxo) and cyclophosphamide (cyclo). **A,** COMPUSYN analysis of 2D 96 well-plate control. **B,** COMPUSYN analysis of 3D ECM microsystem. **C,** Drug screening results for cyclo and doxo in para dosing in 2D control. The blue and orange curves indicate single drug treatments, and the grey curves indicate parallel direction drug combination results. Combination index values are labeled at each data point. **D,** Drug screening results for cyclo and doxo in para dosing in 3D ECM microsystem. **E,** Drug screening results for cyclo and doxo in oppo dosing in 3D ECM microsystem. Experiments were done in triplicates.

Comparison of synergistic and antagonistic combination indeces in 2D and 3D

Analyzing the CI values (**Fig. 4A** and **B**, and placed below each combination data point **Fig. 4C** to **F**), it was noticed that while CI values of 2D and 3D analyses were mostly comparable in para and oppo, some subtle differences stood out. For example, the 2D midpoint CI value for para treatment (doxo and cyclo) started at 0.88 for high doses of doxo and cyclo and decreased to 0.46 for median doses, and then increased to 1.65 for low doses, suggesting better synergism, at midpoint (**Fig. 4C**). Similar trends with a 2.4-fold lower CI value of

0.19 were observed in the para 3D ECM microsystem (Fig. 4D). Importantly, for oppo combinations, maximum synergy occurred at "double-median" dosing in both the 2D control with a CI value of 0.53 and more convincingly in the 3D ECM microsystem with a CI value of 0.19 (Fig. 4E and F). This suggests that the dynamic drug delivery in the 3D ECM microsystem provides a more robust synergy effect compared to the 2D analysis.

To examine a broader applicability of the 3D ECM microsystem, another drug combination common in breast cancer treatment was used: cisplatin and paclitaxel (cis and pac). Unlike the doxo and cyclo

combination, the clinical outcomes using this drug combination are mixed for drug synergy and effectiveness (47, 48). Although one study reported an 85% response rate with the cis and pac combination treatment (49), a response rate of only 21% was found in another similar study (50). As before, drug diffusion profiles were determined for cis and pac individually (Supplementary Fig. S8), before viability and CIs were examined. As shown in Supplementary Fig. S9, similar trends although less distinct were observed as for the doxo and cyclo combination, with a dominance of high cis doses in viability and lower midpoint CIs in the 3D ECM microsystem compared with the 2D control. As expected, given the clinical outcomes mentioned above, CI values were overall higher than found with the doxo and cyclo combination.

Finally, a known antagonistic drug combination (paclitaxel and vincristine) was examined (38, 51). Both combination curves showed significantly different profiles. For the para combination in 2D and 3D

(gray lines in **Fig. 5A** and **B**), the tumor viability was relatively high and stable even with an increasing dose of both drugs, with CI values. In oppo combinations, tissue viability at both ends (high pac or high vin) was lower and only one of the two drugs affected the response as the other drug, as observed in the diffusion simulation (Supplementary Fig. S10), could not effectively diffuse to the far end. This finding is an important distinction compared to the 2D model as in *in vivo* diffusion through the ECM defines drug efficacies and thus the 3D ECM microsystem provides a more accurate resemblance of drug effects.

Comparing then the midpoint para and oppo CI values for these three drug combinations (**Fig. 5E**) showed a stronger synergistic effect for the doxo and cyclo compared with cis and pac, while pac and vin presented an antagonistic effect. The CIs identified for the 3D ECM microsystem were comparable with CIs found in the 2D system. However, 3D CIs demonstrated lower CI values for the syngerstic drug combinations, where the dox and cyclo CI was distinctively lower

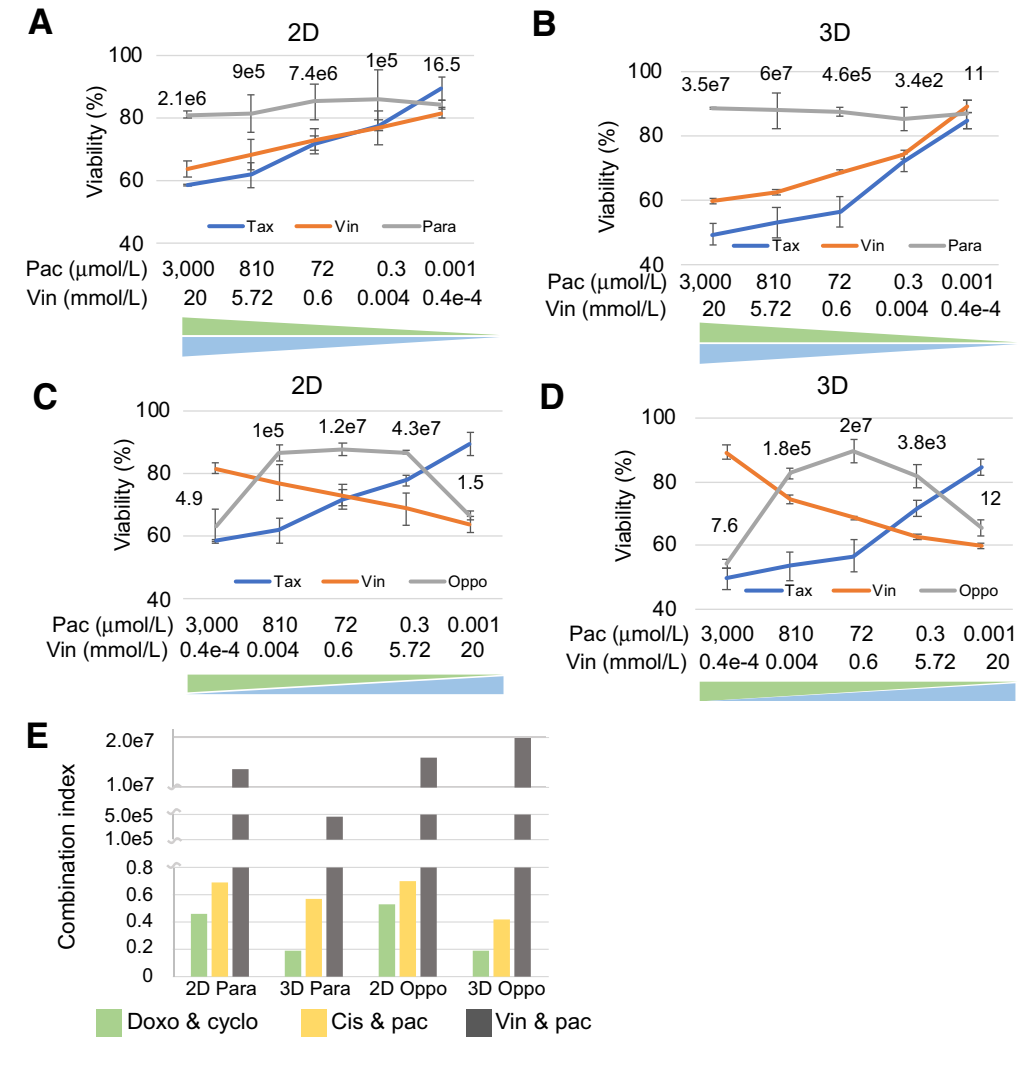


Figure 5.

Comparison of a known antagonistic drug interaction in 2D and the 3D ECM microsystem. **A,** Drug screening results of paclitaxel (pac) and vincristine (vin) in para dosing in 2D 96-well plate control. The blue and orange curves indicate single drug treatments, and the gray curves indicate parallel direction drug combination results. Combination index values are labeled at each data point. **B,** Drug screening results for pac and vin in para dosing in 3D ECM microsystem. **C,** Drug screening results for pac and vin in oppo dosing in 2D control. **D,** Drug screening results for pac and vin in oppo dosing in 3D ECM microsystem. **E,** CI comparison between all three drug combinations (doxo and cyclo, cis and pac, and pac and vin) at double-median dosing.

than the cis and pac CI, compared with the 2D analysis where both CIs appeared similar, thus better reflecting reported success of both combinations in human trials (52).

Discussion

Here, we introduce a novel 3D collagen tumor-on-a-chip approach with microfluidic channels applicable to combinatorial drug screening. The device permits 3D collagen-embedded tumor samples to be rapidly evaluated for drug sensitivy employing drug diffusion profiles from vessel-mimicking channels, which simulate in vivo dynamic drug delivery. Based on mathematical simulations of drug diffusion profiles, local drug concentrations for each tumor sample in the 3D ECM microsystem were determined in a time dependent manner and applied to the 2D controls. Comparison between the 3D ECM microsystem and the commonly used 2D 96-well approach confirmed the appropriateness of the 3D ECM microsystem that provides a much needed physiologically-relevant experimental environment, in determining tissue viability, useful drug ratios and combination indeces. Within a tissue, concentration gradients exist not only for oxygen, pH, nutrients and effector molecules, but also for drugs. Therefore, proximity of a blood vessel, ECM compositions are important factors determining drug concentrations in tumor tissues. As 2D approaches fail to build meaningful gradients, it has long been realized that drug screening in 3D is far superior in high-throughput drug screening; however, cost and limited tissue availability often restrict drug screens in 3D (53). The 3D ECM microsystem presented here helps to overcome these hurdles by offering blood vessel like structures (channels) embedded in collagen and diffusion gradients. Besides single drug gradient generation, we specifically designed and examined parallel dosing and opposite dosing strategies. Thus, the parallel setup mimicked intravenous chemotherapy delivery as a simplified version. As the opposite setup does not represent any in vivo application specifically, it offers an efficient way to test drug combinations in different dose ratios, which can only be achieved by manually adding different doses in parallel. This would require many more devices and tumor tissue pieces. In addition, we presented evidence here that the placement of five tumor pieces in series between two channels enables reliable testing of drug combinations to derive relevant drug ratios and thus, combination indeces.

Adressing tumor heterogeneity through the 3D ECM microsystem

Although 3D cell culture models, such as organoids, allow cell-to-ECM contact, they fail to reflect intratumoral tumor heterogeneity. For example, fibroblasts, adipocytes, immune cells a part of the tumor microenvironment (TME) and modulate the response of cancer cells to chemotherapies and targeted therapies through production of secreted factors (52). Therfore, analyzing tumor tissue that contains all TME cell types is necessary for valuable drug screening. We provide evidence that tumor tissues show decent viability up to 6 days. However, although that can be useful for some research purposes, in drug sensitivity testing such long time periods are not advisable, as prolonged interactions of tumor cells with the collagen scaffold induces cells to migrate out of the tumor that way resulting in different drug responses found in tumors with intact architecture. Another important factor requiring terse analysis time comes from the relative short viability of immune cells ex vivo, compared to cancer cells (54). As we show here in overall tumor viability, future studies are needed to examine individual cell type viabilities in 3D ECM microsystem. Intratumoral heterogeneity is also a result of clonal heterogeneity that influences drug responsiveness and has been addressed by emerging computational prediction models used to optimize cancer therapies (55). Intertumoral heterogeneity which describes genomic differences of the same cancer between two or more patients as well as clonal differences of metastases within one patient, is an equally pressing issue difficult to address in conventional drug screening aproaches (56). Clearly, the 3D ECM microsystem presented here offers a personalized way to screen for effective drug combinations of the tested tissues.

Comparisons of time-dependent effects or dosing frequencies offer important pharmacologic insight into how dosing regimens influence diffusion profiles, drug dosing range, and can lead to variations in drug treatment outcomes. For example, comparisons between the 2D and the 3D ECM microsystem showed that all four different drug application methods generated similar trends with dose-effect patterns in 2D and the 3D ECM microsystem that mostly agreed with each other: fluctuations and curve inflections. However, absolute cell death amounts differed between 2D and 3D, probably due to differences in the actual drug delivery profile over time: constant dosing in 2D versus dynamic dosing 3D. In the control (96-well plates), tumor fragments were soaked in drugs, and thus experienced constant drug dosing, with 12 hours replenishing over a 3-day period. In the 3D device, the tumor fragments were exposed to drugs through diffusion in the 3D ECM microsystem and experienced a dynamic and nonlinearly increasing dose profile, which is physiological more relevant as drug delivery in 2D. Therefore, *in vitro* drug screening by constant dosing is an overly simplified model that provides an inaccurate reference to in vivo drug treatment. With the development of computational models and accuracy in simulations, a more reliable in vitro reference can be provided. Our study is merely a first step in dynamic diffusion simulation, but already presents different drug effects especially in combination index values. For example, our Matlab simulation in 1D applying Fick's second law was a simplified tool to calculate spatiatemperal distribution of all drugs in the device, while a 3D simulation optimized by experimental data are preferrable for more accurate determination in the future.

Other important advantages of the 3D ECM microsystem are: (i) Ease of experimental manipulation: single dosing for the channels for each five-tumors in the device is easier than diluting and combining drug doses multiple times as requied for the traditional 2D approach. (ii) Low drug consumption: the micrometer scaled fluidic system requires only small volumes of reagents. As some drugs (especially new drugs in development) are expensive or initially only synthesized in small batches, our approach provides useful insight early in the drug development process.

In conclusion, we developed an effective and convenient new 3D collagen tumor-on-a-chip approach that offers microfluidic channels to mimic tumor vasculature *in vivo* for drug screening and a cancer appropriate ECM. Our device enables 3D embedded tumor samples to be examined with single/double drug combinations in a physiologically meaningful way as it enables drug diffusion through the ECM, which simulates *in vivo* dynamic drug delivery. The 3D ECM microsystem can be adapted depending on individual ECM requirements, availability of tumor tissues, etc., to provide personalized patient treatment.

Materials and Methods

Tumor preparation

All animal experiments were approved by the University of Pittsburgh IACUC. MDA-MB-231 cells were injected into the mammary

fat pad of 3- to 4-week-old female nude immunocompromised SCID-Beige mice and the tumors were harvested 8 weeks after implantation. The tumors were stored in liquid nitrogen (33). Before drug testing, tumor samples were thawed and immediately sliced with a scalpel into roughly 2 mm³ (1 mm*1 mm*2 mm) fragments. Tumor sections close to the necrotic core and the surface were removed. Each fragment was divided into two 1 mm³ fragments, one for live/dead staining to ensure the fragment had over 70% viability. Fragments that were viable were embedded into the 3D ECM microsystems for drug screening.

Tumor device fabrication

Building off our previous work (57), the device chamber was fabricated by cutting PMMA boards (TAP Plastic, 2.4 cm in thickness) into chamber walls (inner: 40*16 mm, outer: 44*20 mm) through a laser cutting system (Epilog). Then, the chamber was attached to a 50*22 coverslip with optical adhesive (NOA 81, Norland products Inc.). The device was cured with UV for 2 minutes and rinsed with 70% ethanol under UV light for 2 hours, then rinsed twice with $1 \times PBS$ to remove residual ethanol. The gelatin template was prepared as described in our previous work (57), then positioned in the chamber. Three or five tumor samples were placed between the parallel channels, with equal distance between each sample, or any other locations for desired local dosing, based on our 1D simulation. Collagen with 3 mg/mL concentration (10% 10× PBS, high concentration collagen type I with corresponding concentration ratio, 1 N NaOH = 0.023*collagen, and DMEM + 10% FBS) was injected into the chamber and covered the tumor samples. Then, the device was maintained at room temperature for 30 minutes, followed by incubation at 37°C for 30 minutes. The gelatin template was then removed with a syringe.

Doxorubicin drug gradient characterization

Doxorubicin (Selleckchem, in DMSO) was first diluted by DMEM $+\,10\%$ FBS to $100~\mu mol/L$, then injected into the left channel of one blank device (without the presence of tumor samples). The device was next imaged using confocal microscopy. Doxorubicin had an excitation/emission wavelength of approximately 480/560 nm. Images were captured moving spatially across the device from the left channel to right channel, at 1-mm intervals. The average intensity of the images (intensity of doxorubicin fluorescence) was determined through image analysis of the confocal microscope images (Axio Observer Z1 Microscope System, Zeiss). The sample was incubated at $37^{\circ} C$ for 24 hours, then removed and another set of images was capture. A baseline intensity was also determined by imaging a blank device without the doxorubicin injection.

Viability test for tumor samples

Tumors embedded in the device were stained with 100 μL of CalAM + EthD-1 solution (adding droplets directly on top of tumors in the device) for 1 hour, then rinsed with 1× PBS twice (10 minutes each). Next, the device was imaged with a confocal microscope. This test is destructive to tumor samples, so multiple samples were needed for day 0 up to day 6 for viability tests. For tumors cultured in 96-well plates, the media was removed, and 100 μL of CalAM + EthD-1 solution was added per well for 30-minute staining followed by 1× PBS rinse twice (10 minutes each). Then, the tumors were imaged with confocal microscopy. Images were then analyzed with ImageJ (ImageJ. nih.gov) to count green (live) and red (dead) cells. Viability was determined by their ratio.

1D-simulation of the drug profile

To demonstrate the feasibility of the model-based data-fitting approach, we simulated and predicted the diffusion profile of drugs through a simplified 1D diffusion equation (29). Because the double channels in our current design were parallel to each other, the diffusion profile along with the device was approximately parallel as well. We simulated the model by integrating the 1D diffusion equation:

$$\frac{\partial C_i}{\partial t} = D_i(X) \frac{\partial^2 C_i}{\partial x^2}$$

using a fixed time step forward Euler method, and second order center difference approximation to the Laplacian. The simulation used Matlab (ver. R2018b; www.mathworks.com).

```
code:
  clear all:
  range = 40; % length between two parallel channels
  dx = 0.1;% distance interval
  pi = 3.1415;
  C = zeros (1, range/dx); %vector for drug concentration
  dt = 0.001;%time interval
  D = 1.635; %Diffusion coefficient of drug
  coe = D^*dt/(dx^*dx); % diffusion coefficient
  tumorp = [1,100,200,300,400]; %tumor positions
  C(1) = 10;%initial concentration value
  T = 1/dt;
  P = [48]; %time range, 48 indicates 48 hours
  m = 1;
  for i = 1:T^*P(m)
       C(1) = 10; %iteration for initial point,
constant injection; for one time injection, C(1)
= C(1) - D^*dt^*(C(1) - C(2))/dx;
       for j = 2:range/dx-1
           C(j) = C(j) + coe^* (C(j+1) - 2^*C(j) + C(j-1));
%general iteration, Forward Euler
           C(j) = C(j) - 0.000001;
           if C(j) < 0
             C(j) = 0; %ensure concentration stays
positive.
       C(range/dx) = C(range/dx) + D*dt*(C(range/dx))
dx-1)-C(range/dx))/dx; %iteration for endpoint
  for l = 1:5
     tumorC(l) = C(tumorp(l)); %concentration at
each tumor position
  plot(C); %concentration profile
```

Tumor drug testing

Single drug testing

In the device, 30 μ L of doxorubicin (100 μ mol/L) or 4-hydroxycyclophosphamide (Toronto Research Chemicals, dissolved in DMSO, 100 mmol/L) diluted in DMEM + 10% FBS was injected into one channel and the device was stored in a 5% CO₂ 37°C incubator for up to 3 days. Every 12 hours, the device was taken out, the drug was removed from channel, and the media in the channels was replenished with fresh drug solutions. In the 2D 96-well control, 100 μ L of doxorubicin/4-hydroxycyclophosphamide with a designated

concentration was added per well. The samples were stored in the incubator for 3 days. The solutions were refreshed every 12 hours.

Double drug testing

Opposite drug administration in the device: 30 µL of doxorubicin (100 µmol/L) solution was injected into the left channel; then, 30 µL of 4-hydroxycyclophosphamide (100 mmol/L) solution was injected into the right channel. The solutions were refreshed every 12 hours. Parallel drug administration in device: The mixture of doxorubicin (100 µmol/L, final concentration) and 4-hydroxycyclophosphamide (100 mmol/L, final concentration) was injected into the left channel. The solutions were refreshed every 12 hours. Opposite/parallel drug administration in 96-well plates: The mixtures of doxorubicin and 4-hydroxycyclophosphamide with designed concentrations were added per well.

All samples were incubated for 3 days, removed, washed twice with PBS, and stained with CalAM and EthD-1 for viability imaging. The same approach was applied to cisplatin + paclitaxel, and paclitaxel + vincristine drug combinations.

Authors' Disclosures

Carola A. Neumann reports grants from the NIH during the conduct of the study, as well as pending patent applications related to this study. R. Schwartz reports grants from UPMC Enterprises outside the submitted work, as well as a patent for US Patent App. 16/854,378 pending. P.R. LeDuc reports grants from Carnegie Mellon University during the conduct of the study, as well as pending patent applications related to this study. Phil R. LeDuc reports grants from Air

Force Office of Scientific Research, Office of Naval Research, Pennsylvania Department of Health, and National Institute of Health during the conduct of the study, as well as a patent for 3D collagen vascular tumor-on-achip mimetics for dynamic combinatorial drug screening pending. Li Wan, John Skoko, Mei Zhang and Jun Yin report pending patent applications related to this study.

Authors' Contributions

L. Wan: Conceptualization, data curation, software, formal analysis, validation, investigation, visualization, methodology, writing-original draft, writing-review and editing. J. Yin: Data curation, supervision, investigation, methodology. J. Skoko: Data curation, supervision, validation, methodology. R. Schwartz: Conceptualization, software, supervision, investigation, methodology, writing-review and editing. M. Zhang: Resources, supervision, validation, investigation, visualization, methodology. P.R. DeLuc: Conceptualization, resources, supervision, funding acquisition, validation, visualization, writing-review and editing. C.A. Neumann: Conceptualization, resources, data curation, formal analysis, supervision, validation, investigation, visualization, methodology, writing-review and editing.

Acknowledgments

This work was supported in part by the Air Force Office of Scientific Research (FA9550-18-1-0262) P.R. LeDuc, Office of Naval Research (N00014-17-1-2566) P.R. LeDuc, Pennsylvania Department of Health (SAP4100077084) P.R. LeDuc, National Institute of Health (R01AG06100501A1), and National Institute of Health (R56 CA233817) C.A. Neumann and National Institute of Health (NIH/NCI P30 CA047904) C.A. Neumann receives support from UPMC Hillman Cancer Center.

The costs of publication of this article were defrayed in part by the payment of page charges. This article must therefore be hereby marked advertisement in accordance with 18 U.S.C. Section 1734 solely to indicate this fact.

Received October 13, 2020; revised February 15, 2021; accepted March 19, 2021; published first March 30, 2021.

References

- 1. Kumar S, Bajaj S, Bodla RB. Preclinical screening methods in cancer. Indian J Pharmacol 2016;48:481.
- 2. Ohie S, Udagawa Y, Aoki D, Nozawa S. Histoculture drug response assay to monitor chemoresponse. Chemosensitivity: Springer; 2005. p79-86.
- 3. Tibbitt MW, Anseth KS. Hydrogels as extracellular matrix mimics for 3D cell culture. Biotechnol Bioeng 2009;103:655-63.
- 4. Huh D, Hamilton GA, Ingber DE. From 3D cell culture to organs-on-chips. Trends Cell Biol 2011;21:745-54.
- 5. Abbott A. Cell culture: biology's new dimension. Nature Publishing Group; 2003.
- 6. Pampaloni F, Reynaud EG, Stelzer EH. The third dimension bridges the gap between cell culture and live tissue. Nat Rev Mol Cell Biol 2007;8:839.
- 7. Ma H, Xu H, Qin J. Biomimetic tumor microenvironment on a microfluidic platform. Biomicrofluidics 2013;7:011501.
- 8. Loessner D, Stok KS, Lutolf MP, Hutmacher DW, Clements JA, Rizzi SC. Bioengineered 3D platform to explore cell-ECM interactions and drug resistance of epithelial ovarian cancer cells. Biomaterials 2010;31:
- 9. Szot CS, Buchanan CF, Freeman JW, Rylander MN. 3D in vitro bioengineered tumors based on collagen I hydrogels. Biomaterials 2011;32:7905-12.
- 10. Hosseini Y, Verbridge SS, Agah M. Bio-inspired microstructures in collagen type I hydrogel. J Biomed Mater Res A 2015;103:2193-7.
- 11. Wan L, Neumann C, LeDuc P. Tumor-on-a-chip for integrating a 3D tumor microenvironment; chemical and mechanical factors. Lab Chip 2020;20:873-88.
- 12. Sokol ES, Miller DH, Breggia A, Spencer KC, Arendt LM, Gupta PB. Growth of human breast tissues from patient cells in 3D hydrogel scaffolds. Breast Cancer
- 13. Halldorsson S, Lucumi E, Gomez-Sjoberg R, Fleming RMT. Advantages and challenges of microfluidic cell culture in polydimethylsiloxane devices. Biosens Bioelectron 2015;63:218-31.
- Wan L, Skoko J, Yu J, LeDuc P, Neumann C. Mimicking embedded vasculature structure for 3D cancer on a chip approaches through micromilling. Sci Rep 2017;7:16724.

- $15. \ \ Murphy \, SV, \, Atala \, A. \, 3D \, bioprinting \, of \, tissues \, and \, organs. \, Nat \, Biotechnol \, 2014;$ 32:773
- 16. Kolesky DB, Truby RL, Gladman A, Busbee TA, Homan KA, Lewis JA. 3D bioprinting of vascularized, heterogeneous cell-laden tissue constructs. Adv Mater 2014:26:3124-30
- 17. Esch EW, Bahinski A, Huh D. Organs-on-chips at the frontiers of drug discovery. Nat Rev Drug Discovery 2015;14:248.
- 18. Huh D, Torisawa Y-s, Hamilton GA, Kim HJ, Ingber DE. Microengineered physiological biomimicry: organs-on-chips. Lab Chip 2012;12: 2156-64.
- 19. Asghar W, El Assal R, Shafiee H, Pitteri S, Paulmurugan R, Demirci U. Engineering cancer microenvironments for in vitro 3-D tumor models. Mater Today 2015;18:539-53.
- 20. Hachey SJ, Hughes CC. Applications of tumor chip technology. Lab Chip 2018; 18:2893-912.
- 21. Begley CG, Ellis LM. Drug development: Raise standards for preclinical cancer research. Nature 2012;483:531.
- 22. Chang TC, Mikheev AM, Huynh W, Monnat RJ, Rostomily RC, Folch A. Parallel microfluidic chemosensitivity testing on individual slice cultures. Lab Chip 2014: 14:4540-51.
- Skardal A, Devarasetty M, Forsythe S, Atala A, Soker S. A reductionist metastasis-on-a-chip platform for in vitro tumor progression modeling and drug screening. Biotechnol Bioeng 2016;113:2020-32.
- 24. Kolesky DB, Homan KA, Skylar-Scott MA, Lewis JA. Three-dimensional bioprinting of thick vascularized tissues. Proc Natl Acad Sci U S A 2016;113: 3179-84.
- 25. Nguyen D-HT, Stapleton SC, Yang MT, Cha SS, Choi CK, Galie PA, et al. Biomimetic model to reconstitute angiogenic sprouting morphogenesis in vitro. Proc Natl Acad Sci U S A 2013;110:6712-7.
- Bhattacharjee N, Urrios A, Kang S, Folch A. The upcoming 3D-printing revolution in microfluidics. Lab Chip 2016;16:1720-42.
- 27. Fisher B, Anderson S, Wickerham DL, DeCillis A, Dimitrov N, Mamounas E, et al. Increased intensification and total dose of cyclophosphamide in a

- doxorubicin-cyclophosphamide regimen for the treatment of primary breast cancer: findings from National Surgical Adjuvant Breast and Bowel Project B-22. J Clin Oncol 1997;15:1858–69.
- Motlagh NSH, Parvin P, Ghasemi F, Atyabi F. Fluorescence properties of several chemotherapy drugs: doxorubicin, paclitaxel and bleomycin. Biomed Opt Express 2016;7:2400–6.
- Mathews J, Walker RL. Mathematical methods of physics. New York, NY: WA Benjamin: 1970.
- Zhao S, Zhao H, Zhang X, Li Y, Du Y. Off-the-shelf microsponge arrays for facile
 and efficient construction of miniaturized 3D cellular microenvironments for
 versatile cell-based assays. Lab Chip 2013;13:2350–8.
- 31. Müller C, Loman A, Pacheco V, Koberling F, Willbold D, Richtering W, et al. Precise measurement of diffusion by multi-color dual-focus fluorescence correlation spectroscopy. EPL (Europhysics Letters) 2008;83:
- 32. Culbertson CT, Jacobson SC, Ramsey JM. Diffusion coefficient measurements in microfluidic devices. Talanta 2002;56:365–73.
- Lawson DA, Werb Z, Zong Y, Goldstein AS. The cleared mammary fat pad transplantation assay for mammary epithelial organogenesis. Cold Spring Harb Protoc 2015;2015:pdb. prot078071.
- Yuanlong Y, Yanming Y, Fuming L, Yufen L, Paozhong M. Characteristic autofluorescence for cancer diagnosis and its origin. Lasers Surg Med 1987;7: 528–32.
- 35. Croce A, Bottiroli G. Autofluorescence spectroscopy and imaging: a tool for biomedical research and diagnosis. Eur J Histochem 2014;58:2461.
- Abujamra AL. Diagnostic techniques and surgical management of brain tumors. BoD–Books on Demand; 2011.
- 37. Zhang N, Fu J-N, Chou T-C. Synergistic combination of microtubule targeting anticancer fludelone with cytoprotective panaxytriol derived from panax ginseng against MX-1 cells in vitro: experimental design and data analysis using the combination index method. Am J Cancer Res 2016:6:97.
- Chou T-C. Theoretical basis, experimental design, and computerized simulation of synergism and antagonism in drug combination studies. Pharmacol Rev 2006; 58:621–81.
- Chou T-C. Drug combination studies and their synergy quantification using the Chou-Talalay method. Cancer Res 2010;70:440–6.
- 40. Ganz PA, Romond EH, Cecchini RS, Rastogi P, Geyer CE, Swain SM, et al. Long-term follow-up of cardiac function and quality of life for patients in NSABP protocol B-31/NRG oncology: A randomized trial comparing the safety and efficacy of doxorubicin and cyclophosphamide (AC) followed by paclitaxel with ac followed by paclitaxel and trastuzumab in patients with node-positive breast cancer with tumors overexpressing human epidermal growth factor receptor 2. J Clin Oncol 2017;35:3942-8.
- Lori J, Stein T, Thamm D. Doxorubicin and cyclophosphamide for the treatment of canine lymphoma: a randomized, placebo-controlled study. Vet Comp Oncol 2010;8:188–95.

- Cappetta D, Rossi F, Piegari E, Quaini F, Berrino L, Urbanek K, et al. Doxorubicin targets multiple players: a new view of an old problem. Pharmacol Res 2018;127: 4–14.
- 43. Emadi A, Jones RJ, Brodsky RA. Cyclophosphamide and cancer: golden anniversary. Nat Rev Clin Oncol 2009;6:638.
- Bastert G, Voelcker G, Peter G, Schmidt-Matthiesen H, Hohorst H. In vitro assay for cyclophosphamide-sensitivity of human tumours: the effect of 4-hydroperoxy-cyclophosphamide on the incorporation of 3H-uridine into the nucleic acids of human tumour cells (author's transl). Z Krebsforsch Klin Onkol Cancer Res Clin Oncol 1976;85:299–307.
- Alberts DS, Einspahr JG, Struck R, Bignami G, Young L, Surwit EA, et al. Comparative in vitro cytotoxicity of cyclophosphamide, its major active metabolites and the new oxazaphosphorine ASTA Z 7557 (INN mafosfamide). Invest New Drugs 1984;2:141–8.
- Kirson ED, Schneiderman RS, Dbalý V, Tovarys? F, Vymazal J, Itzhaki A, et al. Chemotherapeutic treatment efficacy and sensitivity are increased by adjuvant alternating electric fields (TTFields). BMC Med Phys 2009;9:1.
- Sohn JH, Kim YT, Rha SY, Yoo NC, Roh JK, Kim BS, et al. Paclitaxel and cisplatin combination chemotherapy in pretreated breast cancer. Cancer Res Treat 2003; 35:267–73
- Rosati G, Riccardi F, Tucci A, De Rosa P, Pacilio G. A phase II study of paclitaxel/ cisplatin combination in patients with metastatic breast cancer refractory to anthracycline-based chemotherapy. Tumori 2000;86:207–10.
- Gelmon K, O'reilly S, Tolcher A, Campbell C, Bryce C, Ragaz J, et al. Phase I/II trial of biweekly paclitaxel and cisplatin in the treatment of metastatic breast cancer. J Clin Oncol 1996;14:1185–91.
- Sparano JA, Neuberg D, Glick JH, Robert NJ, Goldstein LJ, Sledge GW, et al. Phase II trial of biweekly paclitaxel and cisplatin in advanced breast carcinoma: an Eastern Cooperative Oncology Group study. J Clin Oncol 1997;15:1880–4.
- Chou T-C, Motzer RJ, Tong Y, Bosl GJ. Computerized quantitation of synergism and antagonism of taxol, topotecan, and cisplatin against human teratocarcinoma cell growth: a rational approach to clinical protocol design. J Natl Cancer Inst 1994:86:1517–24.
- 52. Fisusi FA, Akala EO. Drug combinations in breast cancer therapy. Pharm Nanotechnol 2019;7:3–23.
- Langhans SA. Three-dimensional in vitro cell culture models in drug discovery and drug repositioning. Front Pharmacol 2018;9:6.
- Aref AR, Campisi M, Ivanova E, Portell A, Larios D, Piel BP, et al. 3D microfluidic ex vivo culture of organotypic tumor spheroids to model immune checkpoint blockade. Lab Chip 2018;18:3129–43.
- Metzcar J, Wang Y, Heiland R, Macklin P. A review of cell-based computational modeling in cancer biology. JCO Clin Cancer Inform 2019;3:1–13.
- Skaga E, Kulesskiy E, Fayzullin A, Sandberg CJ, Potdar S, Kyttala A, et al. Intertumoral heterogeneity in patient-specific drug sensitivities in treatmentnaive glioblastoma. BMC Cancer 2019;19:628.
- Wan L, Skoko J, Yu J, Ozdoganlar O, LeDuc P, Neumann C. Mimicking embedded vasculature structure for 3D cancer on a chip approaches through micromilling. Sci Rep 2017;7:1–8.



Molecular Cancer Therapeutics

3D Collagen Vascular Tumor-on-a-Chip Mimetics for Dynamic Combinatorial Drug Screening

Li Wan, Jun Yin, John Skoko, et al.

Material

Mol Cancer Ther 2021;20:1210-1219. Published OnlineFirst March 30, 2021.

Updated version Access the most recent version of this article at:

doi:10.1158/1535-7163.MCT-20-0880

Supplementary Access the most recent supplemental material at:

http://mct.aacrjournals.org/content/suppl/2021/03/24/1535-7163.MCT-20-0880.DC1

Cited articles This article cites 53 articles, 7 of which you can access for free at:

http://mct.aacrjournals.org/content/20/6/1210.full#ref-list-1

E-mail alerts Sign up to receive free email-alerts related to this article or journal.

Reprints and Subscriptions

To order reprints of this article or to subscribe to the journal, contact the AACR Publications Department at pubs@aacr.org.

ns pubs@aacr.org

Permissions To request permission to re-use all or part of this article, use this link

http://mct.aacrjournals.org/content/20/6/1210.

Click on "Request Permissions" which will take you to the Copyright Clearance Center's (CCC)

Rightslink site.